Int. J. Turbo Jet-Engines, Vol. **29** (2012), 269–282 DOI 10.1515/tjj-2012-0018

Numerical Simulation of Tangling in Jet Engine Turbines

David A. Cendón,[1,2] **Borja Erice,**[1,2,*] **Francisco Gálvez**[1,2] **and Vicente Sánchez-Gálvez**[1,2]

[1] Department of Materials Science, Universidad Politécnica de Madrid (UPM), Madrid, Spain

[2] Research Centre on Safety and Durability of Structures and Materials (CISDEM). UPM-CSIC, Madrid, Spain

Abstract. The numerical analysis of certain safety related problems presents serious difficulties, since the large number of components present leads to huge finite element models that can only be solved by using large and expensive computers or by making rough approaches to the problem. Tangling, or clashing, in the turbine of a jet engine airplane is an example of such problems. This is caused by the crash and friction between rotor and stator blades in the turbine after an eventual shaft failure. When facing the study of an event through numerical modelling, the accurate simulation of this problem would require the engineer to model all the rotor and stator blades existing in the turbine stage, using a small element size in all pieces. Given that the number of stator and rotor blades is usually around 200, such simulations would require millions of elements. This work presents a new numerical methodology, specifically developed for the accurate modelling of the tangling problem that, depending on the turbine configuration, is able to reduce the number of nodes up to an order of magnitude without losing accuracy. The methodology, which benefits from the cyclic configuration of turbines, is successfully applied to the numerical analysis of a hypothetical tangling event in a turbine, providing valuable data such as the rotating velocity decrease of the turbine, the braking torque and the damage suffered by the blades. The methodology is somewhat general and can be applied to any problem in which damage caused by the interaction between a rotating and static piece is to be analysed.

Keywords. Finite element, tangling, clashing, cyclic symmetry.

PACS®(2010). 87.10.Kn, 89.20.Bb, 89.20.Ef, 89.40.Dd.

* **Corresponding author:** Borja Erice, Department of Materials Science, Universidad Politécnica de Madrid (UPM), Calle del Profesor Aranguren s/n, 28040, Madrid, Spain;
E-mail: borjaerice@mater.upm.es.

Received: May 3, 2012. Accepted: May 8, 2012.

Nomenclature

$()^*$	Variables in for the equations referred to two paired solids
$()'$	Variables expressed in the rotated reference system $O'X'Y'Z'$
$\dot{x}$	$\frac{dx}{dt}$, first derivative with respect time
$\ddot{x}$	$\frac{d^2x}{dt^2}$, second derivative with respect time
x, X	Scalars. Lower or upper-case italic characters
$\mathbf{x}$	Vectors. Lower-case bold faced characters
$\mathbf{x}, \mathbf{X}$	Tensors. Lower or upper-case italic bold faced characters
$\mathbf{X}$	Matrices. Upper-case bold faced characters
A	Johnson-Cook constitutive relation constant
B	Johnson-Cook constitutive relation constant
$\mathbf{b}$	Body forces
$\mathbf{B}$	Strain matrix
c	Number of cyclic repetitions along one stage
c_f	Decay coefficient for Coulomb based friction formulation
C	Johnson-Cook constitutive relation constant
$\mathbf{d}$	Nodal displacements vector
D_1	Johnson-Cook failure criterion constant
D_2	Johnson-Cook failure criterion constant
D_3	Johnson-Cook failure criterion constant
D_4	Johnson-Cook failure criterion constant
D_5	Johnson-Cook failure criterion constant
$\mathbf{e}_i$	Unit vector in i direction
E	Elastic modulus or Young modulus
$\mathbf{f}_{\text{imp}}$	Impact forces
$\mathbf{f}_{\text{lag}}$	Forces introduced due to the cyclic symmetry constraints
H	Hardening parameter
I	Second order identity tensor
m	Thermal softening exponent. Johnson-Cook constitutive relation constant

$\mathbf{M}$ Lumped masses matrix

n Johnson-Cook constitutive relation constant

n_r Number of rotor blades per cyclic sector

n_{sp} Number of NGVs per cyclic sector

N_r Number of rotor blades in a stage

N_{sp} Number of NGVs in a stage

$\mathbf{N}$ Displacement interpolation matrix

T Temperature

T_r Room temperature

T_m Melting temperature

T^* Homologous temperature

$\mathbf{u}$ Displacement vector

v Relative velocity between slave node and master segment

α Scaling parameter

β Scaling parameter

$\bar{\varepsilon}_p$ Equivalent plastic strain

$\dot{\bar{\varepsilon}}_p$ Equivalent plastic strain rate

$\dot{\varepsilon}_0$ User defined strain rate

$\dot{\bar{\varepsilon}}_p^*$ Dimensionless strain rate

$\bar{\varepsilon}_p^f$ Equivalent plastic strain to failure

μ_d Dynamic friction coefficient

μ_s Static friction coefficient

$\boldsymbol{\sigma}$ Cauchy stress tensor

$\boldsymbol{\sigma}'$ Deviatoric stress tensor

σ^* Stress triaxiality

σ_{eq} Equivalent stress

σ_H Hydrostatic stress

σ_y Yield stress

ρ Density

1 Introduction

Numerical methods are increasingly applied to the analysis of some engineering problems related to safety, of which good examples are car crashworthiness simulations [1–3] and blade containment simulations on airplane turbines [4, 5]. The main reason for this is to reduce the costly experimental tests needed for safety assessment which makes use of simulations, to decrease the number of experimental tests in the design process of machines and structures involving human safety risks, desirable. On some occasions there are even legal obligations which require manufacturers to pass tests for safety demonstration. For example, in the case of blade containment on airplane turbines, aviation regulations [6] prescribe obligatory tests for new turbines in order to prove that (with blade failure during turbine operation) no inner part of the turbine will be ejected outside the engine casing. In these situations, numerical simulations can reduce experimental testing, allowing manufacturers to face such kinds of tests with a high level of confidence in products.

However, on some occasions the problem is too extensive and creates a huge numerical model. The situation is especially difficult when impact problems are present, given that they usually require very small element meshes to avoid mesh dependency on results. Such a small element size, combined with the large scale of the problem, can lead to millions of degrees of freedom. Under these conditions, if there is no possibility of problem simplification, the problem can be only faced by using large and expensive computers, spending large amounts of computing time on running the simulations.

Tangling (or *clashing*, following some authors [7]) is another example of the above mentioned problem. It is caused by the impact between the rotor and the stator of a turbine after suffering a hypothetic shaft rupture (see Figure 1). In Figure 1(a), under normal operating conditions, the turbine is impelled by the exhaust gases leaving the combustion chamber. In the case of shaft rupture (Figure 1(b)), two phenomena happen simultaneously: first, since the turbine is no longer connected to the compressor, no drag force brakes turbine rotation which causes the rotational-velocity to increase out of control; second, the turbine is free to move axially and is pushed towards the nozzle guided vanes (NGVs) (Figure 1(c)) until the rotor and stator collide. The former phenomenon is especially problematic, since uncontrolled rotation velocity can lead to a massive blade failure or disk burst. This is why engine manufacturers provide mechanisms to decrease turbine velocity in the case of shaft failure. Such mechanisms are commonly based on a throttle that closes fuel injection whenever shaft failure is detected. However, a common feeling among manufacturers is that the response time of these mechanisms is not fast enough to solve the problem [8]. Because of this, some manufacturers are at present studying use of the mechanism of collision

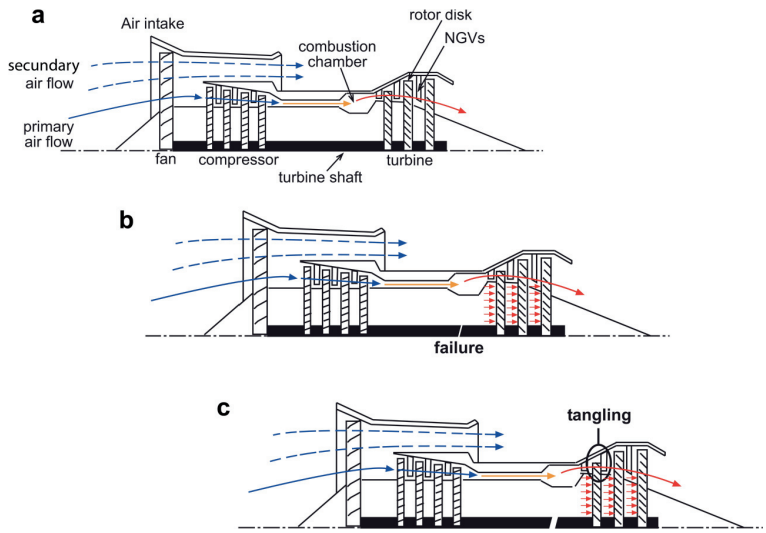

Figure 1. Sequence of the movements inside the turbine in case of shaft failure.

between rotor and stator, after shaft failure, to decrease turbine velocity faster and more safely than any other mechanism. In order to test the capability of this braking strategy, attempts have been made which focus on the numerical simulation of the problem [7, 8] before spending large amounts of money on the development of complex experimental tests for the study of the tangling process.

However, for a realistic simulation of the problem, in the most favourable case, and when one single rotor disk clashes with the nozzle guided vanes of the next stage, both the rotor disk and the NGVs must be included in the numerical simulation. To model accurately the impact between each piece, a small element size is required, leading to meshes of millions of nodes. While some authors have addressed this problem, increasing the element size [7], the results obtained can only be considered a rough approach. This paper presents a novel methodology based on the cyclic symmetry of the problem which, depending on the number of rotor blades and NGVs, can reduce the total number of degrees of freedom up to an order of magnitude without a decrease in precision. The methodology is validated by using a simple example and, finally, applied to the simulation of tangling on an actual jet turbine.

2 The Need for a Methodology to Reduce the Problem

Several numerical methods based on cyclic symmetry can be found in the literature for turbine modelling proposes [9–12]. Most are based on the repetition of the process along time, that is to say, the relative position of a blade regarding its neighbour blades will be repeated again some time later. The basis of these methods is then to model a cyclic sector on a process that is repeated along time and position. Conversely, when impact phenomena are present, all the components considered in the analysis continuously evolve during the tangling process: as they suffer cumulative damage, changes in shape, stresses and temperature, amongst others, it cannot be assumed that any one certain configuration of the turbine will be repeated later. As a result of this, the above mentioned methods cannot be applied.

Before starting the rotation, the problem involves an evident cyclic symmetry (see Figure 2). Depending on the number of rotor blades and NGVs, it is always possible to find a configuration that is repeated cyclically along the

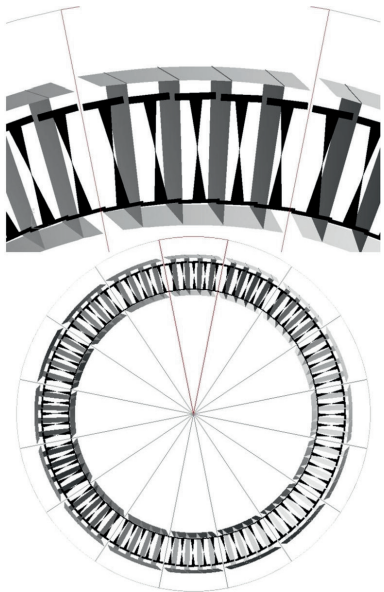

Figure 2. Example of turbine stage with 80 rotor blades (in black) and 64 stator blades (in grey), divided in cyclic sectors (grey lines). The upper detail shows the blades to be included in the smallest possible cyclic sector.

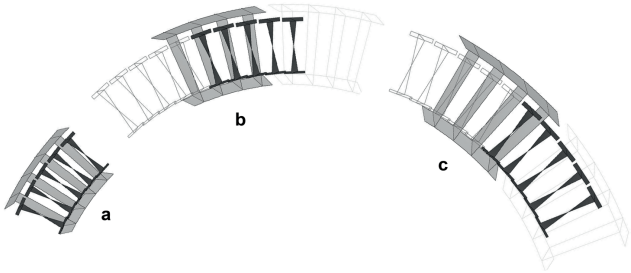

Figure 3. Sequence of the rotation of the cyclic sector. Initial configuration of the sector modelled (a). Sector evolution with the time in (b) and (c).

stage. One stage involves one turbine rotor and the corresponding NGVs. Let N_r be the number of rotor blades of the stage, N_{sp} the number of NGVs in the same stage, n_r and n_{sp} the number of rotor blades and NGVs per cyclic sector and c the number of cyclic repetitions along the stage reads:

$$\begin{aligned} N_r &= n_r c \\ N_{\text{sp}} &= n_{\text{sp}} c \,. \end{aligned} \tag{1}$$

Rearranging each expressions gives:

$$\frac{N_{\text{sp}}}{n_{\text{sp}}} = \frac{N_r}{n_r} = c \,. \tag{2}$$

The maximum simplification would emerge by setting n_r and n_{sp} as small as possible, while c must be the greatest possible. Bearing in mind that N_r, N_{sp}, n_r, n_{sp} and c have to be integer numbers, it can be concluded that c is the maximum common divisor between N_{sp} and N_r. Figure 2 shows an example of a stage with 80 rotor blades ($N_r = 80$) and 64 NGVs ($N_{\text{sp}} = 64$) packed in groups of four (see Figure 2), which makes $N_{\text{sp}} = 16$; the maximum common divisor is then 16. Hence, the smallest cyclic sector must have $16/16 = 1$ NGV and $80/16 = 5$ rotor blades.

However, the cyclic symmetry vanishes as soon as the engine starts to rotate. Figure 3 shows a sequence of the rotation of the cyclic sector: the left picture (a) shows the initial configuration of the sector modelled, while the central (b) and right (c) images show how the sector would evolve along time. Figure 3(b) and Figure 3(c) show how after some rotation (assumed as clockwise) the rotating blades leave the area of interaction with the NGVs included in the sector, as well as how they should be interacting with the following NGVs (contoured with light lines) not present in the model. Moreover, right after the modelled rotating blades, the neighbour blades (contoured with dark lines) should appear to be following them, interacting with the modelled NGVs as well. It is then concluded that a direct use of the cyclic symmetry is not possible.

3 Proposed Methodology

The methodology proposed in this paper uses the cyclic symmetry of the problem, avoiding the problems identified in the previous section. It is based on the use of cyclical symmetry boundary conditions, which are available in most finite element commercial codes, with some modifications explained below.

3.1 Methodology Basis

The methodology basis can be explained by observing Figure 4 and Figure 5. Our model will include the NGVs in the minimum cyclic sector (one NGV, following with our example) and the rotor blades included in the sector (five, in our example), it will additionally include the rotor blades that would be present in the cyclic sector right after the one being modelled (Figure 4). Because of the cyclic symmetry, these blades belonging to the neighbour sector must have continuously the same condition in terms of stresses, deformation and state variables, amongst other variables, as those belonging to the modelled, paired one to one as shown in Figure 4. Moreover, the methodology proposed here connects the rotating blades by cyclic pairs, in such a way that the displacements, stresses, and deformations, amongst others, are shared by the cyclically paired blades. In other words, each blade will suffer the same stresses and deformations, though obviously rotated.

If specific attention is paid to one cyclic pair of rotor blades (in black in Figure 5(a)), the only blade interacting with the NGVs at the beginning of the simulation will be the leading one (on the right of the picture). However, it will "transfer" its condition to the cyclically paired blade suffering the same process as if there were virtual NGVs (contoured with lines) interacting with it. Some time later (Figure 5(b)), it will be the paired blade which will be interacting with the modelled NGV, with the leading blade

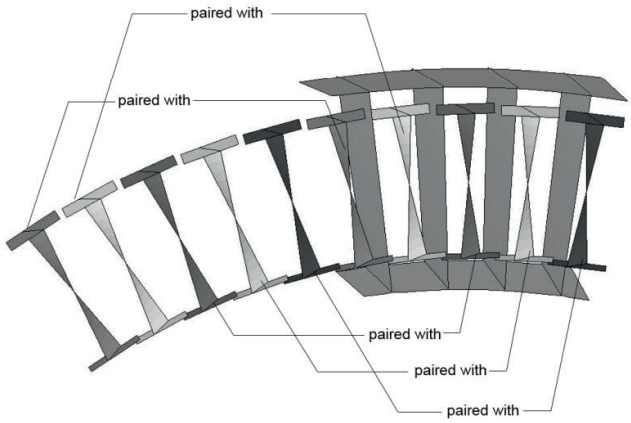

Figure 4. Sketch showing the paired turbine rotor blades in a cyclic sector.

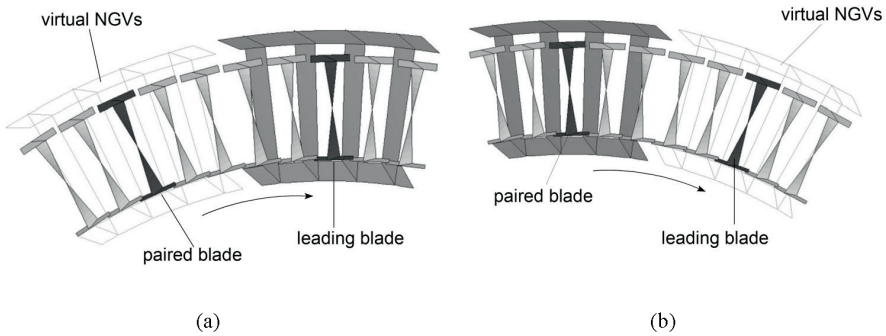

Figure 5. Interaction of the leading blade (in black) of a paired couple of blades with the corresponding NGV (a). Interaction between the paired blade, some time after, with the same NGV (b).

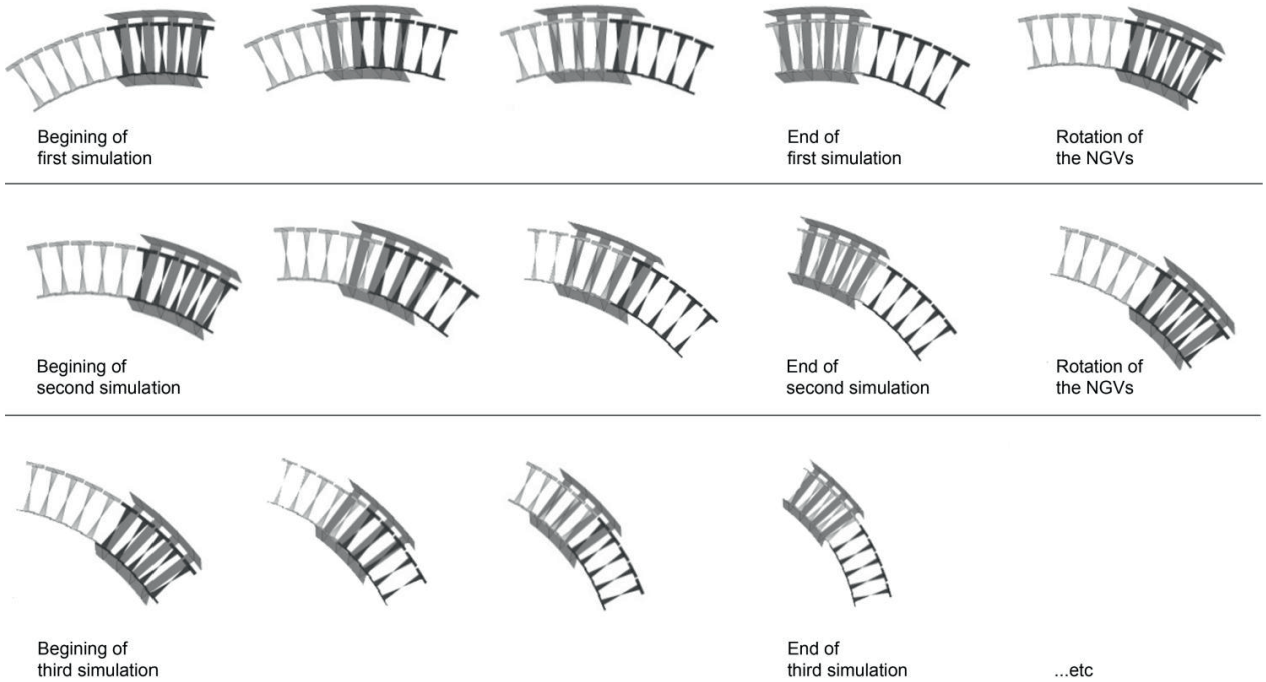

Figure 6. Sketch showing the process in which after each simulation step, the NGVs are rotated to a new position (rotation angle equal to that of the cyclic symmetry), and the simulation is rerun again as many times as desired.

"copying" its condition as if there were behind a virtual NGV present (contoured with lines in Figure 5(b)).

Two additional issues are required for the correct performance of the methodology:

- In Figure 5, it can be appreciated that the simulation cannot be extended beyond the position shown in Figure 5(b). The reason is that new additional blades should be included in the simulation from a third cyclic sector, increasing computational cost. Some procedures must be developed to allow the simulation to continue.
- The real problem to be simulated is the impact between rotor blades and NGVs. Observing once again Figure 5, in the real problem such an impact happens only between one blade and the corresponding NGV (in the position shown in Figure 5(a), between the leading blade and the NGV, while the paired blade should interact with the virtual NGV). However, since in this methodology the leading blades are paired with their cyclically symmetric blades, a mechanism must be provided so that the impact of paired blades behaves as in the impact of one single blade, which is what actually occurs in the real problem.

The first issue can be easily solved by a script which is able to stop the simulation, rotate the stator blade (including its stresses, state variable, and nodal velocities) and rerun the simulation initializing stresses, state variables and nodal velocities on the rotating blades to the same values held at the end of the previous run. This process, which is shown

in Figure 6 must be executed each time the rotating blades have rotated to an angle equal to the angle of cyclic symmetry. This sequence, repeated as many times as needed, can enable the simulation to be extended as much as desired.

The second point, however, requires a deeper analysis which will be addressed in the following section.

3.2 Rotor Blades Cyclic Coupling

The problem is to connect two cyclically symmetric solids in such a way that the connection will behave in exactly the same manner as if they were one single solid. Let a continuum meshed be considered, such as that displayed in Figure 7(a). Focusing on one single finite element of the continuum and using the reference system in Figure 7 as $OXYZ$, the finite element equation of dynamics in the element reads:

$$\mathbf{f}_{\text{imp}} + \int_{\text{vol}} \mathbf{N}^T \mathbf{b} d\,\text{Vol} + \int_{\text{vol}} \mathbf{B}^T \boldsymbol{\sigma}\, d\,\text{Vol} = \mathbf{M}\ddot{\mathbf{d}}\,, \qquad (3)$$

with $\mathbf{f}_{\text{imp}}$ being impact forces vector, $\mathbf{b}$ the body forces vector, $\mathbf{N}$ the displacement interpolation matrix and $\mathbf{B}$ the strain matrix. $\boldsymbol{\sigma}$ is the Cauchy stress tensor expressed as a vector; $\mathbf{M}$ is the lumped masses matrix and $\mathbf{d}$ the nodal displacements vector.

Figure 7(b) shows a meshed solid identical to the single solid considered above and, on its left, a cyclically symmetrical one. Our target will be to pair these two solids in such way that the set will behave as the single solid of Figure 7(a). From a geometrical point of view, a shift can be made from one solid to the other by applying a rotation through the symmetry axis. For this case of the two paired solids, there will now be two equations instead of the single equation (3). The equation for the leading solid will be

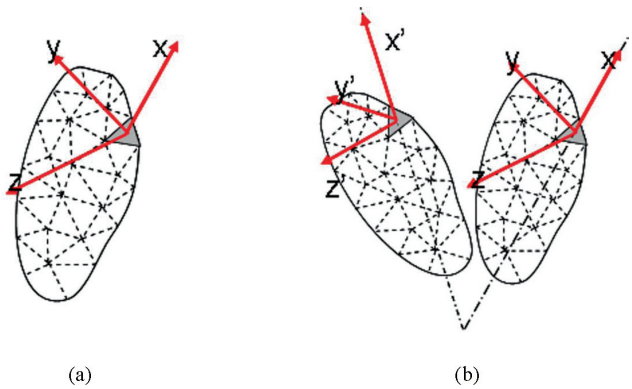

Figure 7. (a) Original continuum meshed and the single finite element (grey) used for the analysis, with its local reference system ($OXYZ$); (b) Coupled continuums, with their coupled finite elements and their local coordinate systems ($OXYZ$ for the original, and $O'X'Y'Z'$ for the coupled one).

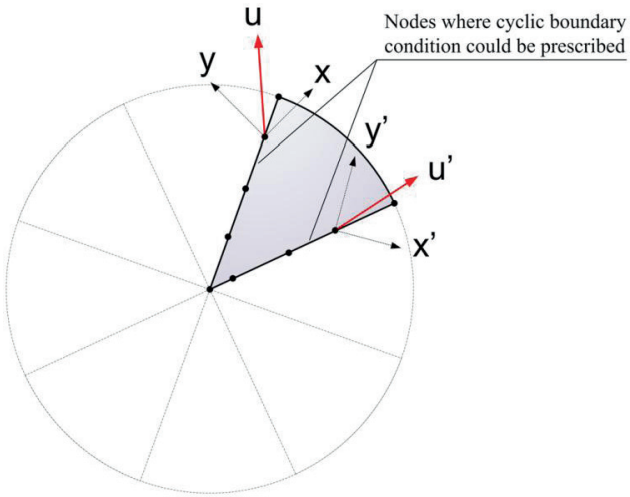

Figure 8. Example of a problem where cyclic boundary condition could be prescribed. Most finite element codes provide such boundary condition option.

expressed again in the $OXYZ$ reference system (equation (4)) while the equation for the trailing paired blade will be expressed in the $O'X'Y'Z'$ rotated system (equation(5)).

$$\mathbf{f}^*_{\text{imp}} + \mathbf{f}^*_{\text{lag}} + \int_{\text{vol}} \mathbf{N}^T \mathbf{b}^* d\,\text{Vol} + \int_{\text{vol}} \mathbf{B}^T \boldsymbol{\sigma}^* d\,\text{Vol} = \mathbf{M}^* \ddot{\mathbf{d}}^*\,, \quad (4)$$

$$\mathbf{f}'^*_{\text{lag}} + \int_{\text{vol}} \mathbf{N}'^T \mathbf{b}'^* d\,\text{Vol} + \int_{\text{vol}} \mathbf{B}'^T \boldsymbol{\sigma}'^* d\,\text{Vol} = \mathbf{M}'^* \ddot{\mathbf{d}}'^*\,. \qquad (5)$$

Equations (4) and (5) are similar to equation (3) with the only difference being the $\mathbf{f}_{\text{lag}}$ term, which represents the forces introduced due to the cyclic symmetry constraints (usually applied by Lagrange multipliers). In this analysis it will be assumed that the leading solid is the only one receiving impact forces, with the reason being the term $\mathbf{f}_{\text{imp}}$ only in equation (3). From now on, the superscript $()^*$ will refer to the equations for the paired solids (in the case of the superscript not being present, the equations refer to the single solid). In addition, the apostrophe $()'$ refers to the variables expressed in the rotated $O'X'Y'Z'$ reference system.

Many finite element codes provide a boundary condition for cyclic symmetries. This boundary condition is intended to model a segment (region with the solid line in Figure 8 of an object that has a rotational symmetry (the whole area in Figure 8, prescribing this boundary condition between nodes on the outer borders of the segment. Such a boundary condition reads:

$$\mathbf{u} \cdot \mathbf{e}_i = \mathbf{u}' \cdot \mathbf{e}'_i\,, \qquad (6)$$

where $\mathbf{u}$ is the displacement of the nodes and is $\mathbf{e}_i$ the i direction unit vector. Equation (6) means that when this equation is prescribed between two cyclical sets of nodes, the displacement vectors components of the leading nodes,

expressed in the $OXYZ$ reference system, are equal to the displacement vectors components of the trailing nodes expressed in the $O'X'Y'Z'$ system.

This cyclic symmetry boundary condition will be used to achieve the purpose. First of all, the condition between all nodal displacements in the leading solid and the trailing one is prescribed. Then, in equations (4) and (5):

$$\ddot{\mathbf{d}}^* = \ddot{\mathbf{d}}'^* . \tag{7}$$

Since the paired solids are equal, with the only difference of being rotated the same angle as the $O'X'Y'Z'$ reference system, the interpolation and the strain matrices must be equal, since they are expressed in their respective reference systems. In the case of the constraint forces vector, the cyclic symmetry implies that both $\mathbf{f}_{\text{lag}}$ and $\mathbf{f}'_{\text{lag}}$ must form a self-balanced forces system. Then:

$$\begin{aligned} \mathbf{N}' &= \mathbf{N} \\ \mathbf{B}' &= \mathbf{B} \\ \mathbf{f}^*_{\text{lag}} + \mathbf{f}'^*_{\text{lag}} &= \mathbf{0} . \end{aligned} \tag{8}$$

Substituting (7) and (8) on (4) and (5), and adding the latter two, we have the dynamics equation for the set of the paired solids:

$$\begin{aligned} &\mathbf{f}^*_{\text{imp}} + \int_{\text{vol}} \mathbf{N}^T \left(\mathbf{b}^* + \mathbf{b}'^*\right) d\,\text{Vol} \\ &\quad + \int_{\text{vol}} \mathbf{B}^T \left(\boldsymbol{\sigma}^* + \boldsymbol{\sigma}'^*\right) d\,\text{Vol} = \left(\mathbf{M}^* + \mathbf{M}'^*\right) \ddot{\mathbf{d}}^* . \end{aligned} \tag{9}$$

Since the same displacements are wanted for the set of paired solids (equation (9)) and the reference single one (equation (3)), the displacements are made equal:

$$\ddot{\mathbf{d}}^* = \ddot{\mathbf{d}} . \tag{10}$$

The impact forces are usually obtained by penalty coefficients applied to the relative displacements between master and slave nodes in contact. Using the same penalty coefficients on the single solid problem than on the paired solids one read:

$$\mathbf{f}_{\text{imp}} = \mathbf{f}^*_{\text{imp}} . \tag{11}$$

Substituting (10) and (11) on (9) we finally obtain:

$$\begin{aligned} &\mathbf{f}_{\text{imp}} + \int_{\text{vol}} \mathbf{N}^T \left(\mathbf{b}^* + \mathbf{b}'^*\right) d\,\text{Vol} \\ &\quad + \int_{\text{vol}} \mathbf{B}^T \left(\boldsymbol{\sigma}^* + \boldsymbol{\sigma}'^*\right) d\,\text{Vol} = \left(\mathbf{M}^* + \mathbf{M}'^*\right) \ddot{\mathbf{d}} . \end{aligned} \tag{12}$$

Equation (12) is the dynamics equation for the paired solids having the same displacements as the reference solid. To make the behaviour of the two paired solids equal to that of the reference solid, equations (12) and (3) are made equal. That leads to:

$$\mathbf{N}^T \left(\mathbf{b}^* + \mathbf{b}'^*\right) + \mathbf{B}^T \left(\boldsymbol{\sigma}^* + \boldsymbol{\sigma}'^*\right) = \mathbf{N}^T \mathbf{b} + \mathbf{B}^T \boldsymbol{\sigma} , \tag{13}$$

$$\mathbf{M}^* + \mathbf{M}'^* = \mathbf{M} . \tag{14}$$

Satisfying equations (13) and (14), two cyclically paired solids that will behave like the original single one are obtained. Equation (14) can be easily satisfied by dividing the density of the reference solid between the cyclically paired solids in such way that the sum of densities of the cyclically paired solids will give the density of the reference one:

$$\rho^* = \alpha\rho ;\ \rho'^* = (1-\alpha)\,\rho \qquad 0 \leqslant \alpha \leqslant 1 . \tag{15}$$

Where ρ is the reference solid density, ρ^* is the density for the leading paired solid ,ρ'^* is the density for the paired trailing solid and α is a real number between 0 and 1. Then, (13) is satisfied, since:

$$\left.\begin{aligned} M^* &= \alpha M \\ M'^* &= (1-\alpha)\, M \end{aligned}\right\} \Rightarrow M^* + M'^* = M . \tag{16}$$

Given that body forces are proportional to density, equation (13) gives:

$$\mathbf{b}^* + \mathbf{b}'^* = \mathbf{b} . \tag{17}$$

Thus, in order to satisfy equation (13) what needs to be satisfied is:

$$\boldsymbol{\sigma}^* + \boldsymbol{\sigma}'^* = \boldsymbol{\sigma} . \tag{18}$$

The latter equation can be satisfied by using a similar decomposition to that in equation (14) by making:

$$\boldsymbol{\sigma}^* = \beta\boldsymbol{\sigma} ;\ \boldsymbol{\sigma}'^* = (1-\beta)\,\boldsymbol{\sigma} \qquad 0 \leqslant \beta \leqslant 1 . \tag{19}$$

With $\boldsymbol{\sigma}$ being the Cauchy stress tensor (expressed as a vector, according to the finite element method terminology) of the reference solid, $\boldsymbol{\sigma}^*$ the Cauchy stress tensor of the leading paired solid, $\boldsymbol{\sigma}'^*$ is the stress tensor of the paired trailing solid and β is a real number between 0 and 1. This decomposition of the stress tensor is possible, since the same displacement on the paired solids is prescribed (expressed in their local coordinate systems). Hence, displacements and strain histories are equal for both solids and for the reference one. Thus, in order to satisfy equation (13) the mate-

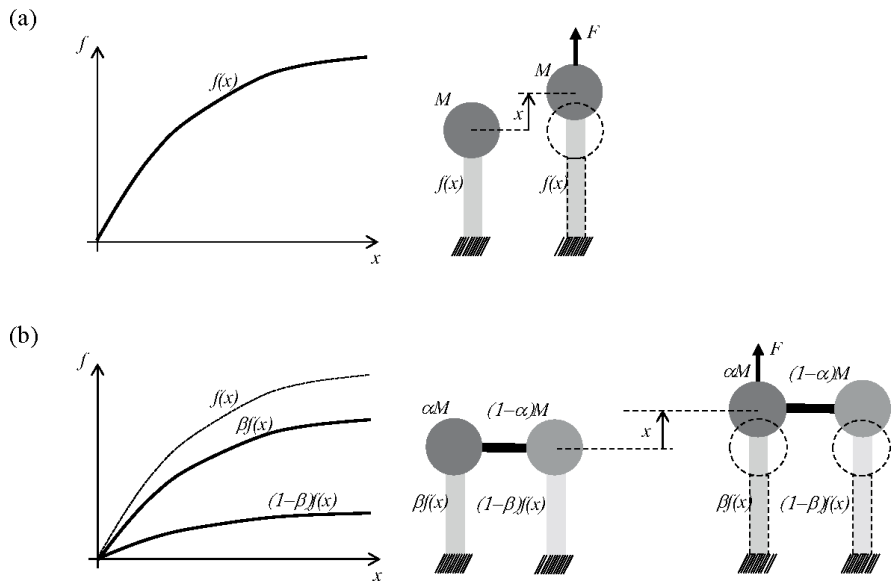

Figure 9. (a) Sketch of the mechanical system of one single mass M attached to a nonlinear bar $f(x)$ used for the example; (b) equivalent system consisting on two masses αM and $(1-\alpha)M$ whose displacements are prescribed to be equal.

rial parameters have to be scaled, that is to say:

$$\left.\begin{aligned} E^* &= \beta E \\ E'^* &= (1-\beta)\, E \end{aligned}\right\};$$
$$\left.\begin{aligned} \sigma_y^* &= \beta \sigma_y \\ \sigma_y'^* &= (1-\beta)\, \sigma_y \end{aligned}\right\}; \qquad (20)$$
$$\left.\begin{aligned} H^* &= \beta H \\ H'^* &= (1-\beta)\, H \end{aligned}\right\}.$$

With E being the Young Modulus, σ_y the yield stress, and H the hardening parameter.

It is noticeable that in equations (16) and (20), the scaling parameters α and β are completely independent and any arbitrary values can be used. Nevertheless, the case of $\alpha = 0.5$ and $\beta = 0.5$ is specially fitting. Here, the physical meaning resembles "dividing the solid in two" with regard to both the mass and the mechanical resistance.

By coupling the solids in the way explained above, not only the behaviour of the coupled solids is equal to the single one: since the equations include the impact forces, if one single element of the set of two paired elements from Figure 7(b) impacts against a certain piece present in the model, the behaviour would be the same as if the element on Figure 7(a) had impacted against the same piece. Given that according to Newton's law impact forces are the same for the impactor and the target, the force felt by the piece that receives the impact is hence the same in each case.

At first view the impact forces being the same for the single solid and for the set of paired ones could be considered as surprising, taking into account that in the case of the paired elements, if only one element impacts against something, its mass is decreased by a factor of α (or $1-\alpha$) and its stress tensor decreased by a factor of β (or $1-\beta$). However, it should be remembered that since the nodes of the paired elements are coupled, if the impact displaces the nodes of one element it must also displace the nodes of its paired element, and that is displacing the total mass of each element. Since the element deformation is paired too, the impact must also mobilise the total strength of the two paired elements.

A simple $1-D$ example of this result is explained as follows. Figure 9(a) shows a punctual mass M attached to the upper end of a bar having a nonlinear behaviour characterised by an $f(x)$ law, where x is the shortening displacement of the bar. The other end of the bar is attached to the ground. If a force F is applied to the punctual mass, the dynamic equation of this system would be given by:

$$F - f\,(x) = M\ddot{x}\,. \qquad (21)$$

Let it be assumed now (Figure 9(b)) two punctual masses αM and $(1-\alpha)M$, the first attached to the upper end of a bar with a nonlinear behaviour given by $\beta f(x)$ and the second attached to the upper end of a nonlinear bar characterised by $(1-\beta)f(x)$. The lower end of each bar is attached to the ground. To prescribe the same movement on each punctual mass is akin to joining them by an infinitely rigid bar. Therefore, if a punctual force F is applied to one of these masses, both masses and both bars must be displaced at the same time.

The dynamic analysis of this system would be represented (Figure 9(c)) by the two mass/bar sets, and an in-

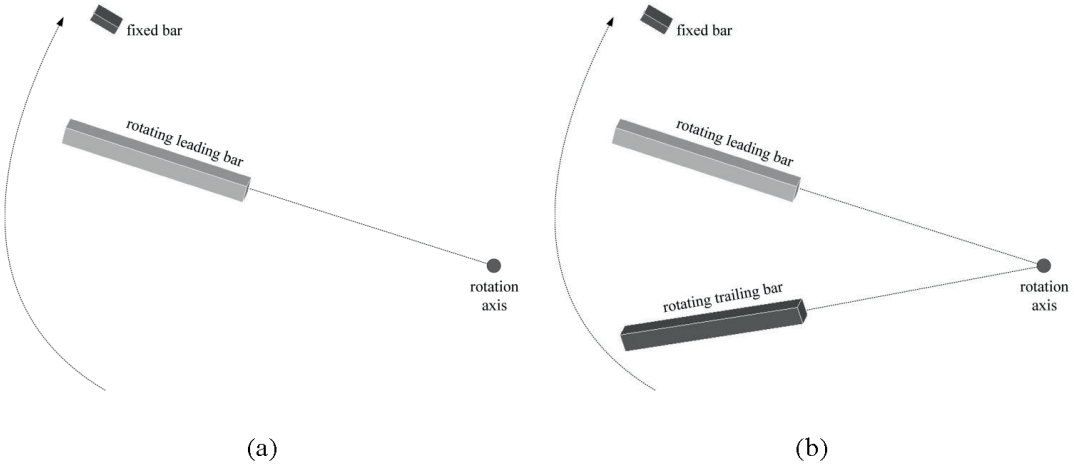

Figure 10. Initial configuration of the finite element models used for validate the proposed methodology.

ternal force F_{int} acting on each mass which would be necessary to prescribe the same displacement on them. Therefore, for this system:

$$F - F_{\text{int}} - \beta f\,(x) = \alpha M \ddot{x}\,, \tag{22}$$

$$F_{\text{int}} - (1-\beta)\,f\,(x) = (1-\alpha)\,M\ddot{x}\,. \tag{23}$$

The variable x is the same in the equations since the displacement has been prescribed to be so. Then, if (21) and (22) are added, the same expression as in equation (21) is obtained:

$$F - f\,(x) = M\ddot{x}\,. \tag{24}$$

Therefore, the set of two punctual masses αM and $(1-\alpha)M$ attached to two bars $\beta f(x)$ and $(1-\beta)f(x)$ respectively, whose displacements are prescribed to be the same, behaves the same as a single mass M attached to a bar $f(x)$. Obviously, the response of the set of the two coupled masses against an external force F is the same as the response of the single mass when subjected to the same force, regardless of the character of this force. If the external force is an impact force the behaviour of each system is the same. In the case of the coupled masses, if a force is applied to one of the two masses, such force will move that mass, but it will also drag the coupled mass, mobilising its inertia (mass) and the strength of its corresponding bar. Subsequently, if the system of one single mass impacts against an external object, the force felt by this object would be the same as if the object had been impacted by one of the masses of the system of coupled masses.

It is important to note that in equations (22) and (23), forces $\beta f(x)$ and $(1-\beta)f(x)$ can be added because they share the same displacement x. Therefore, this addition can be performed whether the behaviour of the bars is linear or not (such an addition is not based on the superposition principle).

In the case of the cyclically paired elements, the practical result of making equations (3) and (12) equal expresses the same idea. Equation (12) is the dynamics equation of the system of cyclically paired elements, sharing the same nodal displacements on their local reference systems, and equation (3) is the dynamics equation of the single element. By making the equations equal, the dynamics law is made equal for the single element and the paired ones, as in equations (21) and (24). If one of the paired elements impacts against a piece its nodes will move; however, they will also drag the nodes of the paired element, mobilising its inertia and strength. As in the case of the simple example shown above, the strength of each element can be added since they share the same nodal displacements in their local coordinate systems, no matter if their constitutive equation is linear or not. Such an extreme is validated in the following section.

4 Validation of the Methodology

In order to test the methodology for pairing solids examined in the previous section, a simple example was simulated using the LS-DYNA nonlinear finite element code [13]. First

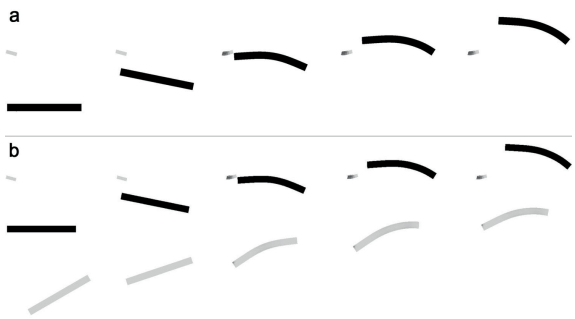

Figure 11. Striking sequences between rotating and fixed bars for a reference case (a) and for the validation case (b).

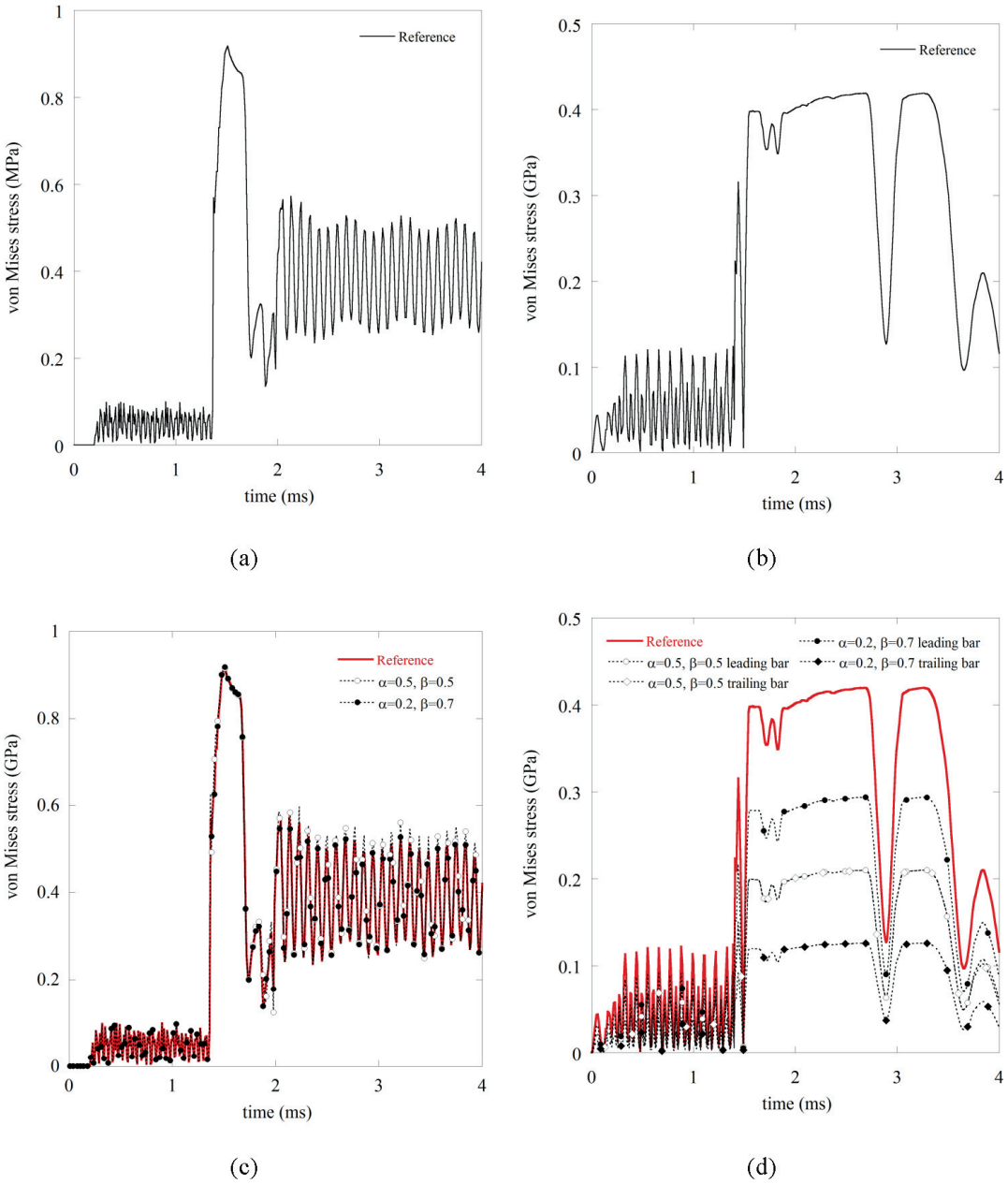

Figure 12. Stress histories for the fixed (a) and rotating bar (b) in the reference calculation. Stress histories for the fixed (c) and rotating bars (d) in the validation calculation with different values of scaling parameters α and β.

of all, a reference case was modelled, consisting of a single rotating bar that struck a small bar fixed on the periphery (see Figure 10(a)). The rotating bar played the role of a rotor blade, while the small bar represented an NGV impacted by the rotor. Next, the same case was modelled but including two paired bars forming a certain angle between them, and coupled using the methodology described in the previous sections (Figure 10(b)).

Eight-node reduced integration hexahedrons were used to model both the reference (one rotating bar) and the validation cases (two rotating bars). In order to prescribe similar movement conditions of a real rotor blade, the subsequent boundary and initial conditions were applied to the reference case:

- In the nodes of the rotating bar end closest to the axis of rotation, the velocity in radial direction was set to zero.
- An initial rotational velocity was imposed to all the nodes of the rotating bar, simulating the rotation of the turbine rotor disk.

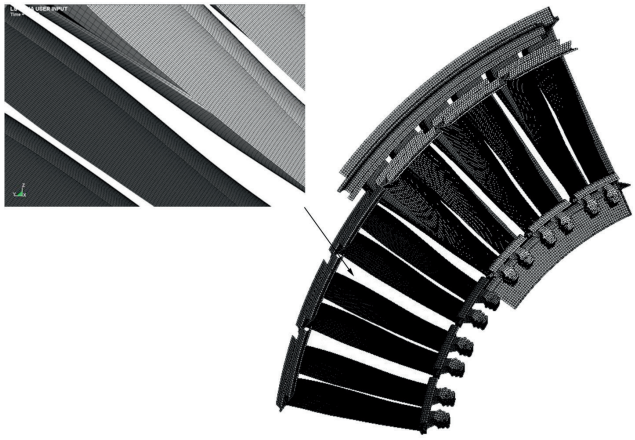

Figure 13. Geometry and mesh used for the rotating blades and the NGVs. The upper left detail shows the element size used.

- The nodes of the left end of the fixed bar were constrained, simulating an NGV fixed to the turbine casing and with no rigid body movement.

In the validation case, the boundary and initial conditions were applied only to the rotating leading bar because cyclic symmetry condition was imposed on the rotating trailing bar. The contact between parts was modelled using the penalty based *AUTOMATIC_SINGLE_SURFACE algorithm available in LS-DYNA [13]. No friction was modelled between parts. The material model was of no importance in these numerical simulations, as the authors were seeking to demonstrate the validity of using the cyclic symmetry condition. Hence, the bars were modelled as an elasto-plastic isotropic material. For this purpose the *MAT_PLASTIC_ISOTROPIC command [13], using random material constants was used.

The sequence of Figure 11(a) shows the rotation of the reference case bar and its deformation after striking the fixed bar. The sequence of Figure 11(b) shows the same striking sequence for the validation case. It can be seen in 12(b) how the rotating trailing bar was deformed when the rotating leading bar struck the fixed short bar. As shown in 12(b), each bar was deformed equally. Moreover, they were deformed in a manner equal to the reference case shown in Figure 11(a).

Figures 13(a) and 13(b) show the histories of stresses (with the von Mises stress against time chosen as an example) obtained in a certain element of the fixed and the rotating bar respectively.

Figure 12(c) shows the stress histories obtained in the same element of the fixed bar shown in Figure 12(a). For the coupled bars using cyclic symmetry condition, different scale factors ($\alpha = \beta = 0.5$ and $\alpha = 0.2$, $\beta = 0.7$ as examples) were used as can be seen in Figure 12(d). It can be appreciated how in each case (reference and validation), the von Mises stress history obtained in the fixed bar were the same between each other and equal to that obtained in the reference case. This result showed how the methodology preserved the stresses obtained in the stroked parts, since the same result was achieved using two solids paired with the methodology proposed here and using one single solid. In the paired bars, however, the same history as in the reference case was obtained, but scaled by the factor β in the rotating leading bar, and by the factor $1 - \beta$ in the rotating trailing bar, according to equation (20). Obviously, in order to obtain the real stress state in the coupled bars, the inverse coefficient ($1/\beta$ in the rotating leading bar, or $1/(1 - \beta)$ in the rotating trailing bar) should be applied.

The methodology proposed in this paper was applied for the tangling analysis on one stage of the low pressure turbine (LPT) of an actual jet engine. The simulations were run in a 2 Intel Quad-Core computer with 4 GB of RAM memory, using LS-DYNA explicit code [13]. Even though it was a relatively common computer, the methodology allowed for simulation of more than 70 ms of the process, modelling both the transient and the stationary phases of the problem. The turbine velocity decrease, as well as the blades failure patterns, were obtained as the main results.

4.1 Finite Element Model

The turbine modelled in this example consisted of 36 rotor blade pairs and 12 NGVs, giving a maximum common divisor of 12. Following the methodology presented in previous sections, it was necessary to model only $12/12 = 1$ NGVs and $36/12 = 5$ rotor blade pairs. Five additional rotor blades, cyclically coupled with the previously mentioned rotor blade pairs, were required following the proposed methodology. The reduction of the turbine components present in the model, due to the methodology, allowed use of a small element size (average size of $1.0 \times 1.0 \times 1.0$ mm^3) without leading to a huge number of elements. Using such an element size, the mesh reached a total number of 717962 nodes and 583254 elements, from which 392364 elements corresponded to the rotor blades and 190890 to the NGVs. If the proposed methodology had not been used, $392364 \times 6 = 2354184$ elements for the rotor blades plus $190890 \times 12 = 2290680$ elements for the NGVs would have been necessary to achieve the same level of mesh resolution. Such resolution was important to analyse the final condition of the blades after 70 ms, since the mesh size in impact phenomena simulations is critical to achieve good results if failure criteria are used [14]. The deformations and failure patterns were then modelled with a high level of spatial resolution.

Because of the particular geometry of the jet engine modelled here, tangling is expected to occur only in one stage of the turbine. This explains why one single stage was included in the model and why the rest of the parts rotating

with the stage were added as discrete mass and moment of inertia (divided by 12).

The cyclic sector of the LPT was modelled by using eight-node reduced integration hexahedrons available LS-DYNA [13]. The thrust of the engine was modelled by applying a prescribed acceleration to the turbine rotor nodes. The acceleration was considered positive in the downstream direction, normal to the rotation plane. This acceleration was calculated by dividing the thrust by the mass of the rotating components of the engine. Note that to achieve the tangling condition, the nodes belonging to the turbine rotor should be free to move in axial direction (normal to the rotation plane). Hence, no constraints were imposed on these nodes in the axial direction. The radial velocity on the nodes belonging to the fir-tree type root of the rotor blades (blade base) was set to zero.

Since the only purpose in these preliminary simulations was to analyse the braking capability of the turbine, no engine torque was included in the model, and the rotor was only submitted to an initial rotating velocity. For deeper analyses, engine torque and aerodynamic considerations could be combined with the methodology presented here.

The contact between all the parts was modelled with a penalty based algorithm using *AUTOMATIC_SINGLE_SURFACE command. All the parts were included in one set part to model the contact. In order to achieve a reasonable braking rate in the rotational velocity of the engine (provided by the manufacturer), the friction coefficients were adjusted. The friction in LS-DYNA is based on Coulomb formulation, where an exponential function interpolates smoothly the

transition between static (μ_s) and dynamic (μ_d) friction coefficients:

$$\mu = \mu_d + (\mu_s - \mu_d)\exp\left(-c_f\,|v|\right)\,, \tag{25}$$

where v is the relative velocity between slave nodes and master segments in contact and c_f is a decay constant. In this case, c_f was set to zero, μ_s to 0.2 and μ_d to 0.2.

4.2 Material Modelling. Johnson–Cook Material Model

The Johnson-Cook (JC) material model [15, 16] is a widely used model for impact and high strain rate phenomena. Most non-linear finite element method codes have the JC model already implemented. It consists of a constitutive relation [15] and a failure criterion [16]. The expressions for the constitutive relation and the failure criterion are uncoupled, which means that no softening effects are included.

The JC constitutive relation is relatively simple and versatile. It models the flow behaviour of the equivalent or von Mises flow stress $\sigma_{\text{eq}} = \sqrt{3J_2} = \sqrt{3/2\boldsymbol{\sigma}' : \boldsymbol{\sigma}'}$, where J_2 is the second invariant of the deviatoric stress $\boldsymbol{\sigma}' = \boldsymbol{\sigma} - 1/3tr\,(\boldsymbol{\sigma})\,I$, $\boldsymbol{\sigma}$ is the Cauchy stress tensor and I is the second-order identity tensor. The expression is formulated by using three independent terms, which scale each other (see eq. (25)). The first one is the strain hardening of the material, the second is the strain rate hardening and the third is the thermal softening. Five material constants are necessary to model the plastic flow of the material. The JC constitutive relation reads:

$$\sigma_{\text{eq}}^{JC} = \left[A + B\bar{\varepsilon}_p^n\right]\left[1 + C\,\ln\dot{\bar{\varepsilon}}_p^*\right]\left[1 - T^{*m}\right]\,, \tag{26}$$

where $\bar{\varepsilon}_p$ is the equivalent plastic strain, $\dot{\bar{\varepsilon}}_p^* = \dot{\bar{\varepsilon}}_p \big/ \dot{\varepsilon}_0$ is the dimensionless plastic strain rate being $\dot{\bar{\varepsilon}}_p$ with $\dot{\bar{\varepsilon}}_p$ being the equivalent plastic strain rate and $\dot{\varepsilon}_0$ a user defined reference strain rate; $T^* = (T - T_r)/(T_m - T_r)$ is the homologous temperature where T is the actual temperature, T_r is the room temperature and T_m is the melting temperature. A, B, n, C and m are the five material constants.

The model computes the temperature increase due to plastic work, assuming adiabatic conditions according to:

$$\dot{T} = \frac{\chi}{\rho C_p}\sigma_{\text{eq}}\dot{\bar{\varepsilon}}_p\,, \tag{27}$$

where χ is the Taylor-Quinney coefficient, ρ is the density and C_p is the specific heat.

The JC failure criterion defines a damage parameter D [16] which is based on the accumulation of the equivalent plastic strain. The evolution of this damage parameter is defined as follows:

$$\dot{D} = \frac{1}{\bar{\varepsilon}_p^f\left(\sigma^*, \dot{\bar{\varepsilon}}_p, T\right)}\dot{\bar{\varepsilon}}_p\,, \tag{28}$$

where $\bar{\varepsilon}_p^f$ is the equivalent plastic strain to failure. The material will fail when the accumulation of equivalent plastic strain reaches the equivalent plastic strain to failure. In other words, the damage variable D will increase until it reaches unity. At this moment the material will fail and the elements will be deleted from the calculation, setting the stress components to zero.

Johnson and Cook [16] proposed an expression of the equivalent plastic strain to fracture as a function of stress triaxiality (σ^*), strain rate and temperature. The stress triaxiality is defined as:

$$\sigma^* = \frac{\sigma_H}{\sigma_{\text{eq}}}\,, \tag{29}$$

where $\sigma_H = 1/3tr(\boldsymbol{\sigma})$ is the hydrostatic stress component of the stress tensor. The equivalent plastic strain to fracture $\bar{\varepsilon}_p^f$ is defined with three separate products. The first term is simply Rice and Tracey's [16] original formula. The second and third are homologous to those defined for the constitutive relation, that is to say, the strain rate and temperature

Physical properties						
E_{RT} (GPa)	ρ (kg/m^3)		ν	C_p(J/kg ºC)	χ	
210	7850		0.3	460	0.9	
Strain hardening			Strain rate hardening		Thermal softening	
A (MPa)	B (MPa)	n	C	$\dot{\varepsilon}_0$ (s^{-1})	m	T_m (ºC)
1035	190	0.3	0.006	5×10^{-4}	4.5	870
Failure criterion						
D_1	D_2		D_3	D_4	D_5	
0.1133	2.11		−1.65	0.0125	0.9768	

Table 1. Johnson-Cook material model constants for FV535 Stainless Steel.

influence on the equivalent plastic strain to failure respectively. The equivalent plastic strain to fracture is expression reads:

$$\bar{\varepsilon}_p^f = \left[D_1 + D_2 \exp\left(D_3\sigma^*\right)\right]\left[1 + D_4 \ln \dot{\bar{\varepsilon}}_p^*\right]\left[1 + D_5 T^*\right], \tag{30}$$

where D_1, D_2, D_3, D_4 and D_5 are material constants.

The material chosen for modelling the turbine rotor and the NGVs was FV535 stainless steel. A series of quasi-static and dynamic tests of smooth and notched specimens performed at various temperatures was necessary to obtain the JC material constants for this steel. The dynamic tests were carried out by using a Split Hopkinson pressure bar [18]. Following the procedure developed by the authors in [19, 20] all the constants were obtained. The physical properties and JC constitutive relation material constants for FV535 stainless steel are summarised in Table 1.

4.3 Results

The facture patterns in rotor blades and NGVs after 70 ms can be seen Figure 14. Figure 15 shows the history of relative rotational velocity of the rotor obtained in the simulations. It should be noted that following the proposed methodology, the total simulation is obtained by a succession of intermediate calculations, and that therefore the final history was obtained by placing the history of each intermediate calculation right after the history of the previous one.

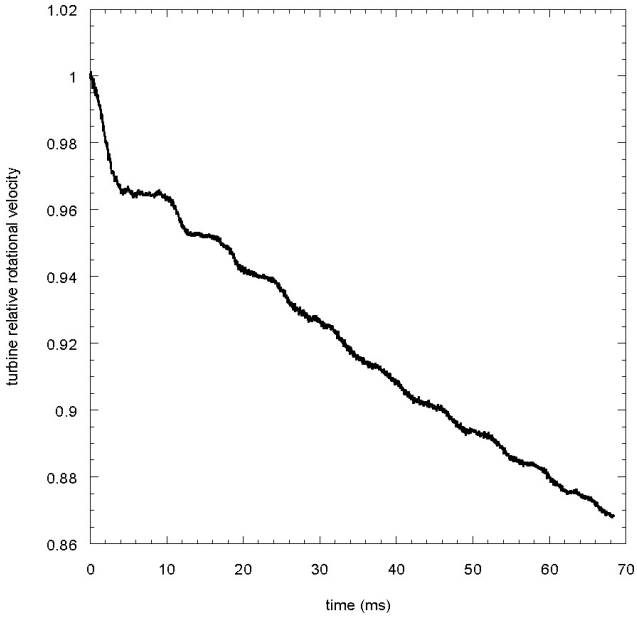

Figure 15. Time history of the relative rotation velocity of the turbine obtained in the simulation.

Figure 14. Final condition of the blades. A high level of resolution in the failure patterns was achieved.

5 Conclusions

The numerical analysis of tangling in jet engine turbines was performed by using a new methodology based on the finite element method. The methodology took advantage of the cyclic symmetry of the problem, reducing the number of degrees of freedom without a decrease on the accuracy of the solution. The reduction of the number of degrees

of freedom achieved depended on the total number of rotor blades and NGVs in one LPT stage. In the case of the turbine considered in this article, the methodology allowed the division of the total number of elements by a factor close to eight.

The methodology, which can be also applied to other engineering problems where rotation, impact and/or wear are involved, allowed the numerical simulation of weighty problems with relatively simple computers. It could be also applied when a high accuracy is desired in the impact and damage processes involved in the problem.

Acknowledgments

The authors would like to express their gratitude to the Spanish Ministerio de Economía y Competitividad, by funding this research through CONSOLIDER-INGENIO programme and through the project with reference BIA2011–24445. Authors would also like to acknowledge to the company Industria de TurboPropulsores ITP for their support and useful comments.

References

[1] Summers, S. M. and Hollowell, W. T., "NHTSA'S crashworthiness modeling activities" National High Traffic Safety Administration, paper #251.

[2] Gholami, T., Lescheticky, J. and Paßmann, R., "Crashworthiness Simulation of Automobiles with ABAQUS/Explicit" 2003 ABAQUS User's Conference. 2003.

[3] Heimbs, S., Strobl, F., Middendorf, P., Gardner, S., Eddington, B. and Key, J., "Crash simulation of an F1 racing car front impact structure" 7th European LS-DYNA conference. 2009.

[4] Gálvez, F., Cendón, D. A., Enfedaque, A. and Sánchez-Gálvez, V., "Materials behaviour and numerical simulation of a turbine blade-off containment analysis" Proceedings of Structures Under Shock and Impact IX. N. Jones and C. Brebbia Eds. WIT press. (2006), pp. 433–444.

[5] Carney, K. S., Pereira, J. M., Revilock, D. M. and Matheny, P., "Jet engine fan blade containment using an alternate geometry" International Journal of Impact Engineering, Vol. 36, Issue 5. (2009). pp. 720–728.

[6] Federal Aviation Administration. Federal aviation regulation part 33, Section 33.94. 1984.

[7] Frola, C., Vassallo, A., Degiovanni, M. and Mattone, M., "Turbine clashing transient analysis: impact of rotor disk stage onto static vane stage after shaft rupture". Proceedings of ASME Turbo Expo 2008: Power for Land, Sea and Air. Berlin, Germany. 2008.

[8] Environmentally Friendly Aero-Engine *VITAL* Project. 6th European Framework Programme. 2002.

[9] Thomas, D. L., Dynamics of rotationally periodic structures. Int. J. Numer. Meth. Eng. 14 (1979), pp. 81–102.

[10] Wildheim, J., Excitation of rotationally circumferentially periodic structures. J. Sound Vib. 75 (3) (1981), pp. 397–416.

[11] Srinivasan, A. V., Vibrations of bladed disks assemblies – a selected survey. J. Vib. Acoust. Stress Reliab. Des., 106 (1984).

[12] Slater, J. C., Forced response of bladed disks assemblies – a survey. The shock and vibration digest 31 (1) (1999), pp. 17–24.

[13] LS-DYNA KEYWORD USER'S MANUAL Version 971, Livermore Software Technology Corporation, Livermore, California, 2007.

[14] Børvik, T., Clausen, A. H., Eriksson, M., Berstad, T., Hopperstad, O. S. and Langseth, M., Experimental and numerical study on the perforation of AA6005-T6 panels, International Journal of Impact Engineering, 32 (2005), pp. 35–64.

[15] Johnson, G. R. and Cook, W. H., A Constitutive Model and Data for Metals Subjected to Large Strains, High Strain Rates and High Temperatures, in: 7th International Symposium on Ballistics, The Hague, 1983, pp. 541–547.

[16] Johnson, G. R. and Cook, W. H., Fracture characteristics of three metals subjected to various strains, strain rates, temperatures and pressures, Engineering Fracture Mechanics, 21 (1985), pp. 31–48.

[17] Rice, J. R. and Tracey, D. M., On the ductile enlargement of voids in triaxial stress fields, Journal of the Mechanics and Physics of Solids, 17 (1969), pp. 201–217.

[18] Kolsky, H., "An investigation of the mechanical properties of materials at very high strain rates". Proc. Royal Soc. B. 62 (1949), p. 676.

[19] Gálvez, F., Cendón, D. A., Enfedaque, A. and Sánchez-Gálvez, V., "High strain rate and high temperature behaviour of metallic materials for jet engine turbine containment" Journal de Physique IV (134), (2007), pp. 1269–1274.

[20] Erice, B., Gálvez, F., Cendón, D. A. and Sánchez-Gálvez, V., "Flow and fracture behaviour of FV535 steel at different triaxialities, strain rates and temperatures". Engineering Fracture Mechanics 79 (2012), pp. 1–17.